Dalton Transactions

Accepted Manuscript

ROYAL SOCIETY OF CHEMISTRY

www.rsc.org/dalton

Synthesis, spectral and thermal studies of pyridyl adducts of Zn(II) and Cd(II) dithiocarbamates, and their use as single source precursors for ZnS and CdS nanoparticles

Damian C. Onwudiwe[1*], Christien A. Strydom[1], Oluwatobi S. Oluwafemi[2], Eric Hosten[3], Anine Jordaan[4]

[1]Chemical Resource Beneficiation (CRB) Research Focus Area, North-West University, Private Bag X6001, Potchefstroom 2520, South Africa

[2]Department of Chemistry, Cape-Peninsula University of Technology, P.O Box 652, Capetown 8000, South Africa

[3]Department of Chemistry, Nelson Mandela Metropolitan University, P.O Box 77000, Port Elizabeth 6031, South Africa

[4]Laboratory for Electron Microscopy, CRB Research Focus Area, North-West University, Private Bag X6001, Potchefstroom 2520, South Africa

* Corresponding author

Email: dcconwudiwe@gmail.com

Tel: +27 18 299 1068

Fax:+27 18 299 2350

Abstract

The synthesis, spectroscopic characterisation, and thermal studies of pyridyl adducts of Zn(II) and Cd(II) complexes of N-ethyl-N-phenyl dithiocarbamate, represented as [ZnL_2py] and [CdL_2py_2], are reported. Single-crystal X-ray structural analysis of the Zn compound showed that it is five-coordinate with four sulphurs from dithiocarbamate and one nitrogen from pyridine in a distorted square pyramidal geometry. The thermogravimetric studies indicate that the zinc and cadmium compounds undergo fast weight loss, and the temperature at maximum rate of decomposition is at 277 ^{o}C and 265 ^{o}C respectively, to give the metal (Zn or Cd) sulphide residues. These compounds were used as single molecule precursors to produce nanocrystalline MS (M =Zn, Cd) after thermolysis in hexadecylamine. The morphological and optical properties of the resulting MS nanocrystallites were investigated using transmission electron microscopy (TEM), scanning electron microscopy (SEM), UV-Vis absorption and photoluminescence (PL) spectroscopy, and powdered X-ray diffraction (XRD). By varying the growth time, the temporal evolution of the optical properties and morphology of the nanocrystals were investigated.

Key words: Nanoparticles; ZnS; CdS; dithiocarbamate complexes; thermolysis;

1. Introduction

The synthesis of II-VI semiconductor nanoparticles (NPs) has become a niche focus area in materials syntheses. This group of compounds continues to generate research interest leading to the development of many synthetic approaches. The major drive is to produce particles in the nanosize regime which are crystalline and regular in both size and shape. ZnS and CdS NPs have been extensively studied among the different II – VI metal chalcogenide semiconductor NPs. [1-6] The reason is mainly due to their nonlinear optical properties and the ability of tuning their band gaps by controlling the NPs size. [7] They have a wide range of applications including light-emitting diodes (LEDs), solid state solar window layers, photoconductors, catalysts, production of hydrogen, electro-luminescent displays, anti-reflection coating for infrared devices and other non-linear optical devices. [8-11] Bulk ZnS crystallizes into two allotropic forms: a cubic form (*c*-ZnS) with sphalerite structure having a band gap of 3.5–3.7eV and a hexagonal form (*h*-ZnS) with wurtzite structure having a band gap of 3.7–3.8 eV. [12] The cubic form is the stable form at room temperature, while at elevated temperatures the wurtzitic (hexagonal) phase becomes more dominant. However, in the nanoscale, the hexagonal phase has been reported at lower temperatures. [13, 14] The stable phase for bulk CdS is the wurtzite form, and this phase undergoes structural transition to the cubic form in the temperature range of 300 – 400 ^{o}C [15]. The hexagonal-cubic phase transition is also size-dependent with a critical transformation size varying from 4 to 15 nm [16-17].

Among the various synthetic methods adopted in the synthesis of II-VI NPs such as wet chemical [18, 19], micro emulsion [20], hydrothermal technique [21], etc., the thermolysis of chalcogenide sources in coordinating solvents also known as single source precursor is a

common and less complex approach. This method allows the effective manipulation of the synthetic conditions, control of the particle growth, and the final morphology. Dithiocarbamate is one of the widely used precursors. Dithiocarbamates exhibit a fast decomposition in their thermal decomposition profile, which is an important factor in single-source precursor method. Thus dithiocarbamate of different groups ranging from heterocyclic [22], alkyl [23], alkyl-phenyl dithiocarbamates [24], are among such that have been used to prepare high quality II-VI nanocrystalline semiconductors.

Herein, we report the syntheses and characterization of two novel precursor complexes, $[ZnL_2py]$ and $[CdL_2py_2]$. These single source complexes of dithiocarbamates were used in the preparation of ZnS and CdS NPs by thermolysing the precursor molecules in hexadecylamine. By varying the growth time, we investigated the temporal evolution of the optical properties and morphology of the as-synthesised nanocrystals

Experimental

Materials

All the chemical reagents used were of analytical grade and were used as received without further purification. Zinc(II) acetate, cadmium(II) chloride, N-ethyl aniline, carbon disulphide, sodium hydroxide were obtained from Sigma Aldrich. Pyridine and chloroform were obtained from Merck.

Physical Properties Measurement

Infrared spectra were recorded on a Bruker alpha-P FT-IR spectrometer in the 500–4000 cm^{-1} range. The NMR spectra were recorded on a 600 MHz Bruker Avance III NMR spectrometer. Microanalyses were carried out using a Elementar, Vario EL Cube, set up for CHNS analysis. The X-ray powder diffraction data were collected on a Röntgen PW3040/60 X'Pert Pro X-ray diffractometer using Ni-filtered Cu K_α radiation (λ= 1.5405 Å) at room temperature. Scanning electron microscopy images were obtained on a Quanta FEG 250 Environmental Scanning electron microscope (ESEM). TEM measurements were performed on a TECNAI G^2 (ACI) instrument operated at an accelerating voltage of 200 kV. The thermal behaviour of the adducts was studied using the simultaneous thermal analysis (SDTA) technique for parallel recording of TG (thermogravimetry) and DSC (differential scanning calorimetry) curves. The study was performed on a SDTQ 600 Thermal instrument. Samples were contained within alumina crucibles and heated at a rate of 10 $^oC\ min^{-1}$ from room temperature to 700 ^oC under flowing nitrogen. The absorption measurements were carried out using a PerkinElmer Lambda 20 UV–vis spectrophotometer at room temperature. A PerkinElmer LS 55 luminescence spectrometer was used to measure the photoluminescence spectra of the nanoparticles.

X-ray crystallography

X-Ray diffraction studies were performed at 200 K using a Bruker Kappa Apex II diffractometer with graphite monochromated Mo K_α radiation (λ = 0.71073 Å). APEXII [27] was used for data collection and SAINT [27] for cell refinement and data reduction. The structure was solved by direct methods using SHELXS-97 [28] and refined by least-squares

procedures using SHELXL-97 [28] with SHELXLE [29] as a graphical interface. Platon [30] and Ortep-3 [31] were used to prepare material and diagrams respectively for this publication.

All non-hydrogen atoms were refined anisotropically. C-bound H atoms were placed in calculated positions and refined as riding atoms with C—H 0.95 (aromatic CH), 0.99 (CH_2), 0.98 (CH_3) Å and with U(H) = 1.2 (1.5 for methyl) U_{eq}(C). The H atoms of the methyl group were allowed to rotate with a fixed angle around the C—C bond to best fit the experimental electron density (HFIX 137 in the SHELX program suite [28]). The structure was refined as a 2-component inversion twin and the dithiocarbamate ethyl group is disordered in a 0.688(9): 0.332(9) ratio. Table 1 contains the crystallographic and refinement parameters.

The data was corrected for absorption effects using the numerical method implemented in SADABS [27]. CCDC 935369 contains the supplementary crystallographic data for this paper.

General synthesis procedures

The parent complexes were prepared as reported earlier [25], and the adducts were prepared by refluxing the respective precursor complex in a pyridine solution and recrystallizing them in a hot chloroform solution as reported earlier [26]. In a typical procedure, approximately 1.2 g of bis (N-ethyl-N-phenyldithiocarbamate)M(II) [M=Zn and Cd] was added to 15 mL pyridine. The mixture was refluxed at a temperature between 80 and 85 ^{o}C for 2 h. The pyridine solution was filtered off and the solid precipitate was rinsed with water followed by ethanol and then recrystallized from hot choloroform.

(Pyridyl)bis(N-ethyl-N-phenyl dithiocarbamato)zinc(II): [ZnL_2py]. The compound was obtained as a white solid. Yield: 1.28 g, (91 %), M.p. 189 - 191 °C. ^{1}H NMR ($CDCl_3$) δ = 7.40 –

7.24 (m, $–C_6H_5$), 1.64 (t, $–CH_3$), 4.20 (q, $–CH_2$), 8.94 (d), 7.84 (t), 7.45 (q) (pyridine). ^{13}C NMR ($CDCl_3$) δ 144.94, 129.27, 128.05, 126.93 ($–C_6H_5$), 53.78($–CH_2$), 12.41($–CH_3$), 149.39, 138.33, 124.61 (pyridine), 207.49 (NCS_2). Selected IR, υ (cm^{-1}): 1443 (C=N), 1260 (C_2-N), 972 (C=S). Anal. Calc. for $C_{23}H_{25}N_3S_4Zn$ (537.07): C, 51.43; H, 4.69; N, 7.82; S, 23.88. Found: C, 51.04; H, 4.81; N, 7.80; S, 23.89. The product was recrystallized from a chloroform/ethanol solution to afford crystals suitable for X-ray crystallography

(Bis-Pyridyl)bis(N-ethyl-N-phenyldithiocarbamato)cadmium(II):[CdL_2py_2]. The compound was obtained as a white solid. Yield: 1.21 g, (88 %), M.p. 249 - 252 °C. ^{1}H NMR (DMSO) δ = 7.31 – 7.22 (m, $–C_6H_5$), 1.14 (t, $–CH_3$), 4.11 (q, $–CH_2$), 8.55(d), 7.78 (t), 7.40 (q) (pyridine). ^{13}C NMR (DMSO) δ 146.27, 129.47, 127.89, 127.09 ($–C_6H_5$), 55.01($–CH_2$), 12.35($–CH_3$), 149.71, 138.42, 124.34 (pyridine), 207.74 (NCS_2). Selected IR, υ (cm^{-1}): 1443 (C=N), 1265 (C_2-N), 985 (C=S). Anal. Calc. for $C_{28}H_{30}N_4S_4Cd$ (663.24): C, 50.70; H, 4.56; N, 8.45; S, 19.34. Found: C, 51.11; H, 4.52; N, 8.12; S, 19.78.

Synthesis of hexadecylamine (HDA) capped ZnS nanoparticles. In a typical procedure, 0.45 g of the precursor complex, [ZnL_2py], was dispersed in 6.0 mL of tri-n-octylphosphine (TOP). The solution was injected into 6.0 g hot hexadecylamine (HDA) in a three-necked flask at 280 °C. The temperature dropped by approximately 20 °C, and the solution turned to a whitish colour. The temperature was gradually increased to 280 °C, and the reaction was allowed to stabilize at this temperature. Aliquots of the samples were taken at 30 min intervals. Addition of excess anhydrous methanol to the solution resulted in the reversible flocculation of the nanoparticles. The flocculate was separated by centrifugation, and dispersed in toluene to give a whitish solution of HDA–capped ZnS nanoparticles.

Synthesis of hexadecylamine (HDA) capped CdS nanoparticles. 0.45 g of the [CdL_2py_2] complex was dissolved in 6.0 mL of TOP. The solution was injected into 6.0 g of hot HDA in a three-necked flask at 268 °C. The solution turned to a yellowish colour and a drop in temperature of 20 °C was observed. The reaction was allowed to stabilize at 268 °C. Aliquots of samples were taken and precipitated with an excess methanol. The precipitate was separated by centrifugation, and dispersed in toluene to give yellowish HDA-capped CdS nanoparticles.

Result and Discussion

Characterization of precursor compounds

The precursors [ZnL_2py] and [CdL_2py_2] were prepared by refluxing a solution of the parent complexes, Zn(II) bis (N-ethyl-N-phenyl dithiocarbamates) and Cd(II) bis (N-ethyl-N-phenyl dithiocarbamates) separately, in excess pyridine at 80 - 85 °C for 2 hours. The chemical reactions proceed as shown in the Eq. (1) and (2). The adducts are soluble in warm chloroform and tetrahydrofuran, and are stable in air under room temparature conditions.

$$ZnL_2 + py_{(excess)} \longrightarrow ZnL_2py \quad \text{..... (1)}$$

$$CdL_2 + py_{(excess)} \longrightarrow CdL_2py_2 \quad \text{..... (2)}$$

Where L = bis (N-ethyl-N-phenyl dithiocarbamate), and py = pyridine.

Description of crystal structures

Pyridyl bis(N-ethyl-N-phenyl dithiocarbamate) Zn(II) [ZnL_2py] (Figure 1) is five coordinate with a distorted square pyramidal geometry. There are two bidentate dithiocarbamate

ligands and one monodentate pyridine ligand. The two dithiocarbamate ligands are symmetry arranged around a two-fold rotational axis. The Zn atom lies towards the pyridine ligand 0.7450 (2) Å above the plane formed by the four sulphur atoms of the two dithiocarbamate ligands. The Zn-S bond lengths are 2.3583(15) Å and 2.6047(17) Å and the Zn-N bond length is 2.061(3) Å. The two dithiocarbamate ligands form two Zn1, S1, S2, C1 planes with an acute angle of 47.16(6) ˚ with each other and 72.07(7) Å with the pyridine plane. The phenyl group on the dithiocarbamate ligand makes an acute angle of 73.11(16) ˚ with the Zn1, S1, C1, S2 plane. There is one long intramolecular H bond C2---H2A…S2 of 2.67 Å. There are two C23---H23…π ring interactions of 2.69 Å with the two Zn1, S1, C1, S2 planes. The crystal packing is shown in Figure 2. Selected crystal data, collection and refinement parameters are summarized in Table 1, and selected bond distances and angles are presented in Table 2.

IR studies

The IR spectra of compounds [ZnL_2py] and [CdL_2py_2] showed evidence for the formation of the dithiocarbamate groups. The thioureide bands appeared at 1433 and 1443 cm^{-1} for the [ZnL_2py] and [CdL_2py_2] complexes respectively. The band is intermediate between the stretching vibrations of the C-N single bonds, at 1250-1350 cm^{-1} and C=N double bonds at 1640-1690 cm^{-1}, suggesting partial double bond character and, therefore, partial delocalization of π−electron density within the dithiocarbamate group[32]. The band also showed a lower value compared to the parent compound (1454 – 1456 cm^{-1}) [25], and it is attributed to the change in coordination number from 4 (in the parent complex) to a higher coordination number: 5 and 6, (after adduct formation), which affect the degree of

interaction between the dithiocarbamate ligands and the metal ion leading to a reduction in the vibrational frequency. It is also due to the transfer of electrons from the nitrogen of the pyridine ligand to the metal ion, thus, enriching the metal electron density upon the adduct formation [34]. The ν(C–S) bands appear around 980 cm^{-1} in all the complexes, without any splitting, supporting the bidentate coordination of the dithiocarbamate to the metal centre [35]. Bands due to the pyridine molecule are masked by those due to dithiocarbamate ligand.

NMR Studies

The chemical shifts of the pyridine group are between 7.40 and 8.94 ppm, and overlapped with the signals due to the phenyl protons observed between 7.40 and 7.22 ppm. The signals due to the methylene protons and the protons of the terminal methyl group of the ethyl substituent appeared as quartet and triplet around 4.20 and 1.15 ppm respectively. The observed deshielding of the methylene and methyl protons on the nitrogen atom is attributed to the release of electrons on the nitrogen of the NRR' (R = ethyl, R' = phenyl) group, forcing high electron density toward the sulphur (or) the metal via the thioureide π-system [36]. All the signals due to the protons in $[ZnL_2py]$ were observed at a lower field compared to $[CdL_2py_2]$. The ^{13}C NMR spectra of the complexes show one sharp singlet signal at 207 ppm which is ascribed to the carbon of the N-CS_2 moiety. The down field shift of the NCS_2 moiety may be attributed to an increase in π-bond character or delocalization of an electron along the C-N bond contributed by the unshared electron pair in the nitrogen atom [37], and an electron donating effect by the ethyl substituents. In addition, the signals for the carbons of methyl and methylene groups connected directly to the N atoms appear at 55 and 12 ppm respectively. The compounds also exhibit the expected signals due to the carbons of aryl groups at 126 – 146 ppm.

Thermal studies

The thermal analyses (TGA and DSC) were conducted to evaluate the thermal behaviour of the complexes, and ascertain the temperature of decomposition. The TGA/ DTG and DSC curves of the complexes are presented in Figure 3 and the results are tabulated in Table 4. The TGA/DTG curve of [ZnL_2py] (Figure 3 a) showed that the decomposition started at 150 °C, and continued till 185 °C. 14.80 % of the sample was lost, which corresponds to the pyridine molecule (calc: 14.70 %). The TGA/DTG curve of [CdL_2py_2] shows almost the same behaviour with [ZnL_2py] but with the loss of two molecules of pyridine (calc: 23.8 %, found: 23.1 %), and the expulsion of the pyridine molecules occurred at lower temperatures (66 – 142 °C). The second stage of decomposition shows a weight loss of 78.7 % and 71.4 % for [ZnL_2py] and [CdL_2py_2] respectively, and subsequently leaving behind residues which corresponds to their respective metal sulphides. It is observed that the temperature at maximum rate of decomposition of the adducts are lower compared to that of the parent complexes: [ZnL_2], 321 °C; [CdL_2], 333 °C [38]. The reason could be the dimeric nature of the parent complexes [33]. The introduction of a Lewis base (pyridine), destroys the dimeric nature resulting in monomeric adducts, thereby lowering the temperatures at maximum rate of decomposition. The DSC curves of both complexes exhibit three endotherms. The first, low-temperature peak corresponds to the release of the pyridine molecule at approximately 176 °C and 107 °C for [ZnL_2py] and [CdL_2py_2] respectively. The second endotherm is the melting temperature, and the third endotherms are attributed to the thermal decomposition of complexes resulting in the metal sulphides.

Characterization of the nanoparticles

Optical Properties

The UV-Vis spectra of the ZnS and the CdS nanoparticles grown at 280 and 268 ^{o}C respectively are shown in Figure 4. All the spectra show a blue shift in their band edge compared to the value of their respective bulk, ZnS (345 nm) and CdS (512 nm) [39]. This blue shift is associated with an increase in the band gap energy and the manifestation of quantum confinement. The spectra of the ZnS nanoparticles indicate that the absorption edge shift to a higher wavelength as the growth time increased. Similarly, the spectra of the CdS nanoparticles show a shift of the characteristic shoulder to higher wavelength. The typical CdS shoulder was evidenced between 474 and 500 nm, as the growth time increased from 30 to 90 min.

Figures 5 (a) and (b) show the photoluminescence spectra of the ZnS and CdS nanoparticles respectively, after different growth times. The spectra also confirm the general trend, i.e the shifting of the emission to higher wavelengths as the reaction time increased. The enhancement of the maximum emission wavelength position with increase in the nanoparticle size is a well-known phenomenon [40, 41]. The PL spectra for the ZnS nanoparticles (Figure 2a) shows two types of emission - a stronger peak at around 320 nm and a weaker and broader peak at around 406 nm. In a colloidal ZnS semiconductor, the photo-excited carriers (electrons and holes) typically recombine with each other through various recombination paths such as direct band-to-band recombination, shallowly trapped recombination via lattice vacancies, and deeply trapped recombination via surface vacancies [42]. The stronger peak at 320 nm (3·87 eV) could be related to the UV excitonic emission [43], while the blue emission at 406 nm (3.05 eV) can be ascribed to vacancies or surface states (SS). A broad blue emission (centered at 430-450 nm) has been reported for the ZnS

nanoparticles generated in situ within the meso-porous material [44]. Peaks in the emission spectrum between 400 - 600 nm are generally suggested to originate from the surface defect states such as sulphur vacancies located at the surface of ZnS nanoparticles [45, 46]. The emission spectra for CdS NPs show band edge luminescence. The emission maxima increased from 375 nm after 30 min growth time, to 387 nm after 60 min, and 404 nm after 90 min growth time indicating an increase in the particle size. A small blue emission of CdS in Figure 5b at around 530 nm has been attributed to surface defect states.

Structural Properties

The TEM images of the as-synthesized ZnS and CdS nanoparticles and corresponding size distributions at different reaction times are shown in Figures 6 and 7 respectively. Figure 6(a) indicates that the ZnS particles are small and spherical at the beginning of the reaction. This grows into larger, well dispersed particles as the reaction time increased. The size distribution has been fit using a Gaussian function, and the average particle diameters were estimated from the peak position. The average particle diameter, as determined from the TEM images are 4.17 ± 0.95 nm (60 min) and 4.83 ± 1.16 nm (90 min) for ZnS NPs. The TEM results indicate an increase in particle size as the growth time increased. The increase in the average particle diameter as the reaction time increased is in agreement with Ostwald ripening. The larger particles would grow by mass transferred due to dissolution of smaller particles. The process corresponds to a decrease of the surface free energy when large particles developed at the expense of smaller particles [47]. Similar observation was reported in our earlier study [48]. The results also confirmed that larger particles are produced at higher reaction time. The TEM images of the CdS NPs (Figure 7) show that larger particles, produced at the beginning of the reaction, breakdown slightly into smaller particles with

narrow size distribution as the reaction time increased. The average particle diameter as determined from the TEM images for CdS NPs are 6 .92 ± 1.52 nm (30 min), 6.08 ± 0.24 nm (60 min) and 6.04 ± 1.28 nm (90 min). The TEM images for CdS NPs also shows the presence of elongated particles (short rods), which could be attributed to the phenomenon of oriented attachment or self-assembly. The presence of these rods is proposed to be responsible for the large shift of the CdS NPs absorption and emission spectra to higher wavelength as the reaction time increased. This shift in the absorption and emission spectra of the elongated particles to higher wavelengths, as compared to the spherical particles has been previously reported by Wang et al., [49]. The authors attributed this increase to the fact that the band gap of the elongated particles depends on both their width and length even though it is more sensitive to their width. The result obtained for CdS NPs is contrary to the one obtained for the ZnS NPs, where smaller particles are produced at the beginning of the reaction. The reason for this difference may be the different precursors used however, more detailed work is ongoing to ascertain this.

The SEM images of the synthesized ZnS and CdS nanoparticles at lower and higher growth times are presented in Figures 8 and 9 respectively. The SEM results show a stack of platelets at shorter reaction time (30 min) which graduates to clusters of particles with amorphous shape at longer reaction time (90 min).

Figure 10 shows the typical powdered XRD (p-XRD) pattern of the ZnS and CdS nanoparticles. ZnS nanoparticles mostly synthesized by colloid chemistry usually have a cubic -zinc blende (sphalerite) structure, C-ZnS, which is a stable phase at low temperatures for ZnS. On the other hand, hexagonal (wurtzite) phase, H-ZnS, is the higher temperature

polymorph of sphalerite, and can be formed at temperatures higher than 1023 °C [50]. There are only a few reports, where pure H-ZnS nanocrystals were obtained with either special solvo-thermal reactions or modified colloid chemistry methods or single-source molecular precursor routes at temperatures below 500 °C [50-54]. The broad nature of the XRD diffraction peaks in Figure 10 indicates the high nanocrystalline nature of the particles. The XRD pattern of the ZnS NPs (Figure 10 (a)) show diffiraction peaks at 2θ values of 25.7, 28.5, 31.2, 40.5, 47.5, 53.0 and 56.5° corresponding respectively to the (100), (002), (101), (102), (110), (103), and (112) crystalline planes of hexagonal ZnS. Similar to ZnS NPs, the CdS NPs (Figure 10 (b)) show peaks at 2θ values of 25.2, 26.5, 28.0, 43.6, 48.6, and 51.7° corresponding to the (100), (002), (101), (110), (103), and (112) crystalline planes of hexagonal CdS. In our earlier study, using Zn(II) bis(N-ethyl-N-phenyl dithiocarbmate) as precursor molecules, we obtained H-ZnS with sizes less than 3 nm at 200 °C [48]. This shows that these types of precursors are excellent material to produce hexagonal ZnS NPs at low temperature.

Conclusion

(Pyridyl)bis(N-ethyl-N-phenyl dithiocarbamato)zinc(II): $[ZnL_2py]$, and (Bis-Pyridyl)bis(N-ethyl-N-phenyldithiocarbamato)cadmium(II):$[CdL_2py_2]$ compounds were synthesized. The single crystal X-ray structure of the $[ZnL_2py]$ compound shows a zinc atom bonded to four sulphur atoms from each dithiocarbamato ligand, and one nitrogen atom from the pyridine ligand. Thermal decomposition studies gave a weight loss resulting in the respective metal chalcogenides. The compounds were effective as single molecule precursors for hexadecyl amine capped ZnS, and CdS nanoparticles. The optical absorption of the as-synthesized particles showed blue shifted band edges with hexagonal wurtzite structure. The TEM

analysis showed that small spherical nanoparticles with an average particle diameter that is < 7 nm are produced with the presence of short nanorods for CdS NPs.

Acknowledgments

This work was supported by National Research Foundation (NRF), South Africa, and North-West University, Potchefstroom, South Africa. Any opinion, findings and conclusions or recommendations expressed in this material are those of the author(s) and therefore NRF does not accept any liability in regard thereto.

Supplementary data

CCDC 935369 contains the supplementary crystallographic data for compound (1). These data can be obtained free of charge via www.ccdc.cam.ac.uk/data_request/cif or from the Cambridge Crystallographic Data Centre, 12 Union Road, Cambridge CB2 1EZ, UK; fax: (+44) 1223-336-033; or e-mail: deposit@ ccdc.cam.ac.uk.

References

[1] D. C. Onwudiwe, C. Strydom, Mater. Lett. 2013, **92**, 71.

[2] T. Trindade, P. O'Brien, N. L. Pickett, Chem. Mater. 2001, **13**, 3843.

[3] Z. Li, J. Ma, Y. Zong, Y. Men, J. Alloy Compd. 2013, **39**, 559.

[4] M. Afzaal, M. A. Malik, P. O'Brien, New J. Chem. 2007, **31**, 2029.

[5] X. Fang, L. Zhang, J. Mater. Sci. Technol. 2006, **22**, 721

[6] D. C. Onwudiwe, C.A Strydom, Oluwafemi Oluwatobi, New J. Chem. 2013, **37**, 834.

[7] A. L. Abdelhady, M. A. Malik, P. O'Brien, J. Inorg. Organomet. Polym, 2013, DOI 10.1007/s10904-013-9902-1

[8] J. Jie, W. Zhang, I. Bello, C. Lee and S. Lee, Nano Today 2010, **5**, 313.

[9] R. Mach, G. Muller, J. Cryst. Growth, 1990, **86**, 866.

[10] T. Yamaguchi, Y. Yamamoto, T. Tanaka, A. Yoshida, Thin Solid Films, 1999, **344**, 516.

[11] X. Fang, T. Zhai, U. K. Gautam, L. Li, L. Wua, Y. Bando and D. Golberg, Prog. Mater. Scie. 2011, **56**, 175.

[12] M. Ahmad, K. Rasool, Z. Imran, M. A. Rafiq, M. M. Hasan, Electronics, Communications and Photonics Conference (SIECPC), Saudi International (2011) doi: 10.1109/SIECPC.2011.5876907

[13] X. Fanga, T. Zhai, U. K. Gautamb, L. Li, L.Wua, Y. Bando , D. Golberg, Prog. Mater. Scie. 2011, **56**, 175.

[14] X. Chen, H. Xu, N. Xu, F. Zhao, W. Lin, G. Lin, Y. Fu, Z. Huang, H. Wang, M. Wu, Inorg. Chem. 2003, **42**, 3100.

[15] R. J. Bandaranayake, G. W. Wen, J. Y. Lin, H. X. Jiang, C. M. Sorensen, Appl. Phys. Lett. 1995, **67**, 831.

[16] C. Ricolleau, L. Audinet, M. Gandais, T. Gacoin, J.P. Boilot, M. Chamarro, J. Cryst. Growth 1996, **159**, 861.

[17] N. Bao, L. Shen, T. Takata, K. Domen, A. Gupta, K. Yanagisawa, C. A. Grimes, J. Phys. Chem. C 2007, **111**, 17527.

[18] N. Dixit, H. Soni, M. Chawda and D. Bodas, Mater. Lett. 2009, **63**, 2669.

[19] S. Ramesh, V. Narayanan, Chem. Sci. Trans. 2(S1) 2013, S192.

[20] J. Zhang, B. Han, J. Liu, X. Zhang, G. Yang and H. Zhao, J. Supercrit. Fluids, 2004, **30**, 89.

[21] T. T. Q. Hoa, L. V. Vu, T. D. Canh, N. N. Long, J. Physics, 2009, **187**, 012081.

[22] T. Mthethwa, V.S.R. Rajasekhar Pullabhotla, P. S. Mdluli, J.Wesley-Smith, N. Revaprasadu. Polyhedron 2009, **28**, 2977.

[23]. M. Lazell, S. J. Nørager, P.O'Brien, N. Revaprasadu, Mater. Sci. Eng., C 2001, **16**, 129.

[24] D. C. Onwudiwe, P. A. Ajibade. Mater. Lett. 2011, **65**, 3258.

[25] D. C. Onwudiwe, P. A. Ajibade Polyhedron 2010, **29**, 1431.

[26] D. C. Onwudiwe, C. A. Strydom, E. Hosten, Inorg. Chimica Acta. 2013, **401**, 1.

[27] Bruker (2007). *APEXII, SAINT, SADABS*. Bruker AXS Inc., Madison, Wisconsin, USA.

[28] G. M. Sheldrick. *Acta Cryst.* 2008, **A64**, 112.

[29] C. B. Hübschle, G. M. Sheldrick, B. Dittrich. J. Appl. Cryst. 2011, **44**, 1281.

[30] A. L. Spek, J. Appl. Cryst. 2003, **36**, 7.

[31] L. J. Farrugia, J. Appl. Cryst. 1997, **30**, 565.

[32] S.P. Sovilj, G. Vuˇckovi´, K. Babi´, T.J. Sabo, S. Macura, N. Jurani´, J. Coord. Chem. 1997, **41**, 19.

[33] D.C. Onwudiwe, P. A. Ajibade, B. Omondi, J. Mol. Struct. 2011, **987**, 58.

[34] F. Jian, Z. Wang, Z. Bai, X. You, H. Fun, K. Chinnakali, I.A. Razak, Polyhedron 1999, **18**, 151.

[35] F. Bonati, R. Ugo. J. Organometal. Chem., 1967, **10**, 257.

[36] P. J. Rani, S. Thirumaran, S. Ciattini, Phosphorus, Sulfur, and Silicon and the Related Elements, 2013, **188**, 778.

[37] R. Nomura, A. Takabe, H. Matsuda, Polyhedron 1987, **6**, 411.

[38] D.C. Onwudiwe, P. A. Ajibade, Int. J. Mol. Sci. 2012, **13**, 9502.

[39] D.C.Onwudiwe, T.P.J.Krüger, C.A.Strydom, Mater. Lett. 2014, **116**, 154.

[40] M. Nirmal, L. Brus, Acc. Chem. Res. 1999, **32**, 407.

[41] X. Michalet, F. Pinaud, T.D. Lacoste, M. Dahan, M. P. Bruchez, A. P. Alivisatos, S. Weiss, Single Mole. 2001, **2**, 261.

[42] W-S. Chae, J-H. Yoon, H. Yu, D-J. Jang, Y.-R. Kim, J. Phys. Chem. B 2004, **108**, 11509

[43] Y. Jiang, X.M. Meng, J. Lui, Z.Y. Xie, C.S Lee, S.T. Lee, Adv. Mater. 2003, **15**, 323.

[44] W.-H. Zhang, J.-L. Shi, H.-R. Chen, Z.-L. Hua, D.-S. Yan, Chem. Mater. 2001, **13**, 648.

[45] W. G. Becker, A. J. Bard, J. Phys. Chem. 1983, **87**, 4888.

[46] W. Chen, Z. Wang, Z. Lin, L. Lin, J. Appl. Phys. 1997, **82**, 3111.

[47] F. Antolini, E. Burresi, L. Stroea, V. Morandi, L. Ortolani, G. Accorsi, M. Blosi, J. Nanomater. 2012, **2012**, 815696.

[48] D. C. Onwudiwe, C. Strydom, O. Oluwatobi , S. P. Songca, Mater. Res. Bull. 2012, **47**, 4445.

[49] Q.Wang, D. Pan, S. Jiang, X. Ji, L. An, B. Jiang, J. Cryst. Growth 2006, **286**, 83

[50] Y. Zhao, Y. Zhang, H. Zhu, G. C. Hadjipanayis, J. Q. Xiao, J. Am. Chem. Soc. 2004, **126**, 6874.

[51] W. Liu, Mater. Lett. 2006, **60**, 551.

[52] Y. Dong, Q. Peng, Y. Li, Inorg. Chem. Commun. 2004, **7**, 370.

[53] Q. Zhao, L. Hou, R. Huang, Inorg. Chem. Commun. 2003, **6**, 971.

[54] Z. Qiao, G. Xie, J. Tao, J. Solid State Chem. 2002, **166**, 49.

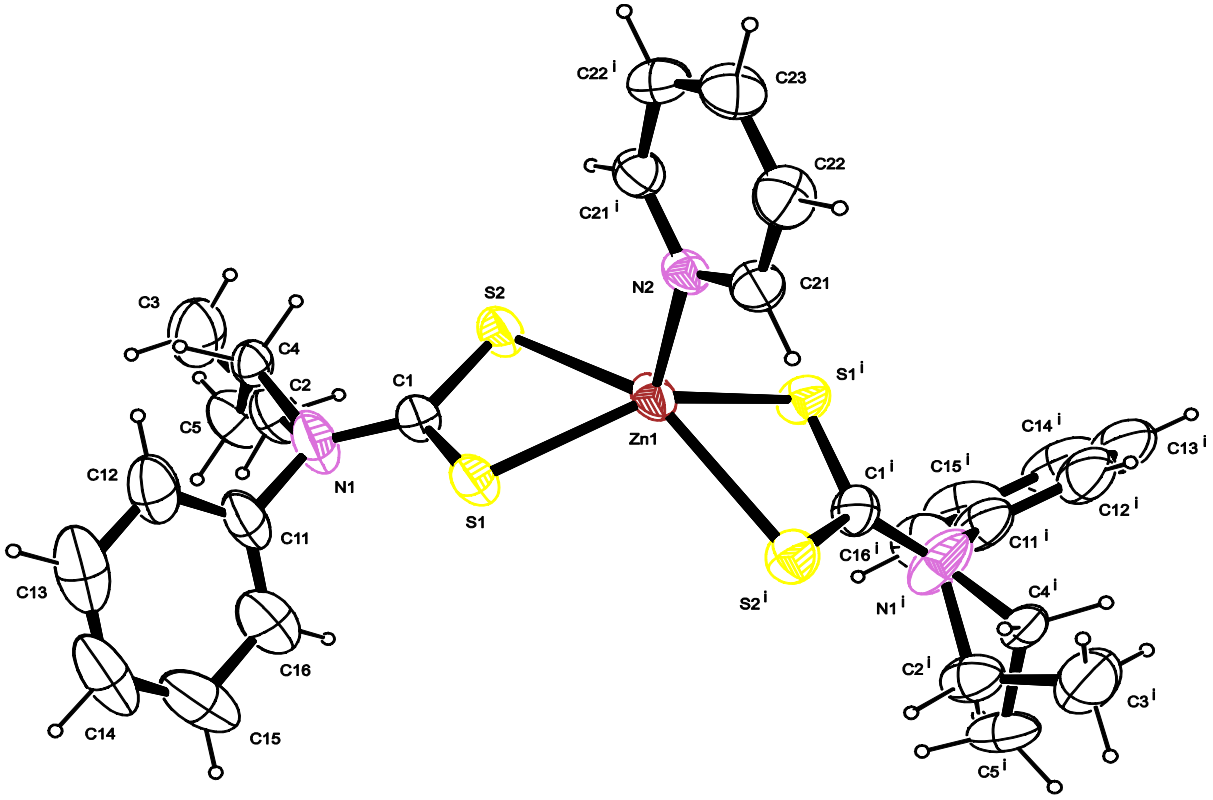

Figure 1. The molecular structure of Pyridyl bis(N-ethyl-N-phenyl dithiocarbamate) Zn(II), [ZnL_2py], with displacement ellipsoids drawn at a 50 % probability level. Symmetry element i: y, x, -z.

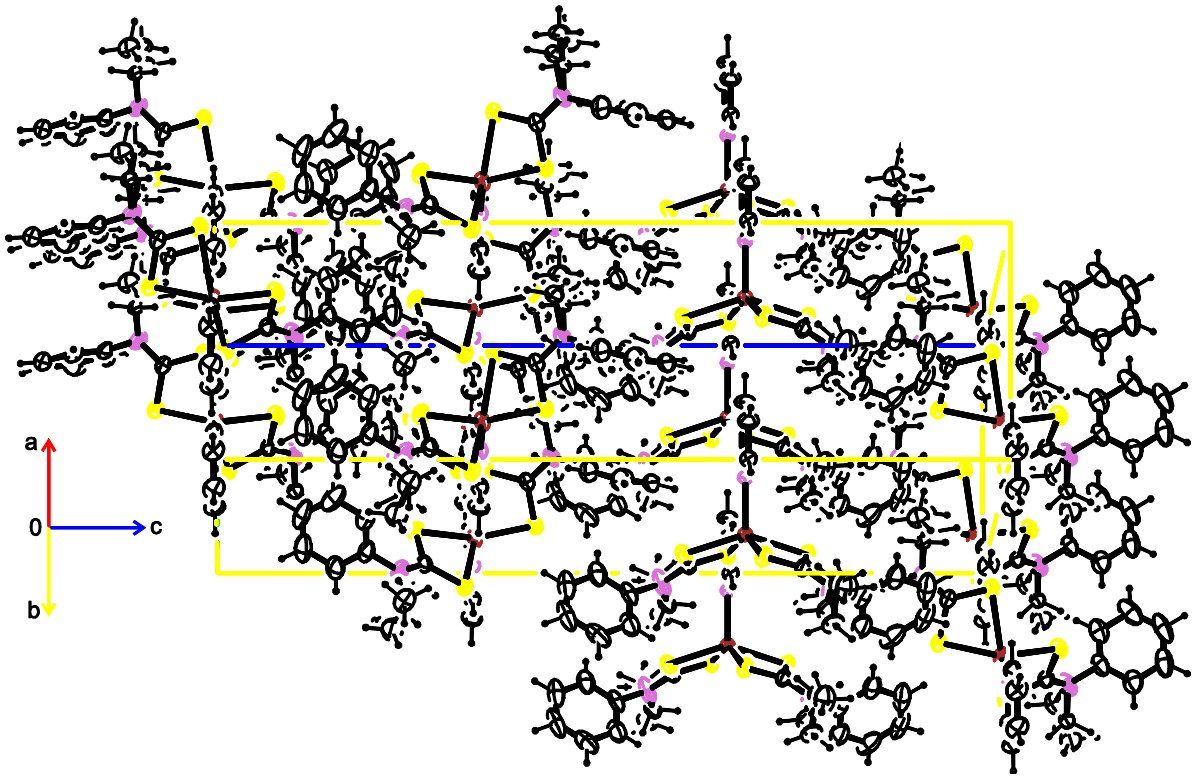

Figure 2. Crystal packing of Pyridyl bis(N-ethyl-N-phenyl dithiocarbamate) Zn(II) [ZnL_2py] viewed normal to the a axis.

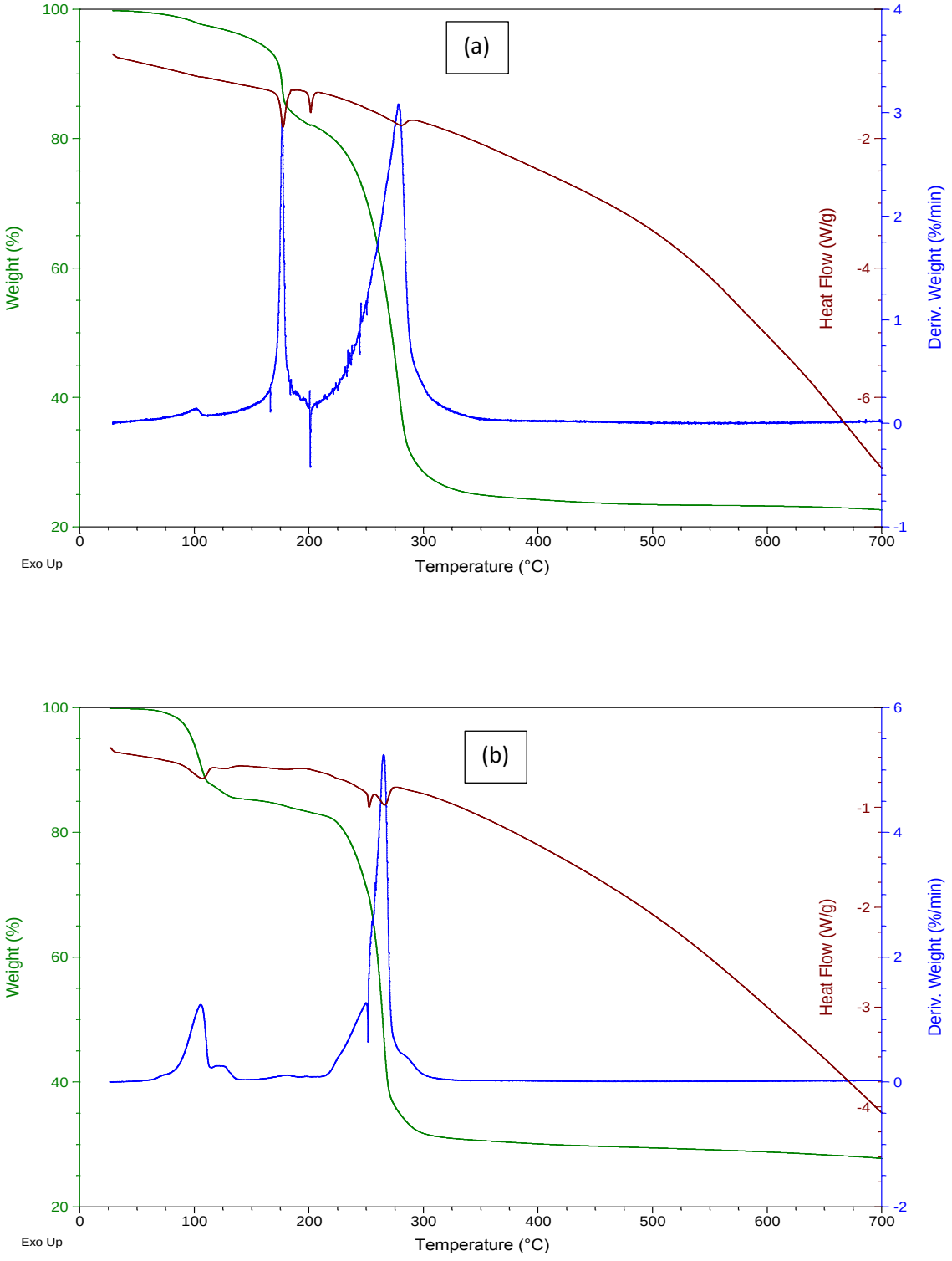

Figure 3. TG/DTG and DSC curves of compounds (a) [ZnL_2py], and (b) [CdL_2py_2] obtained under a nitrogen atmosphere (75 mL/min) and heating rate of 10 ^{o}C/min.

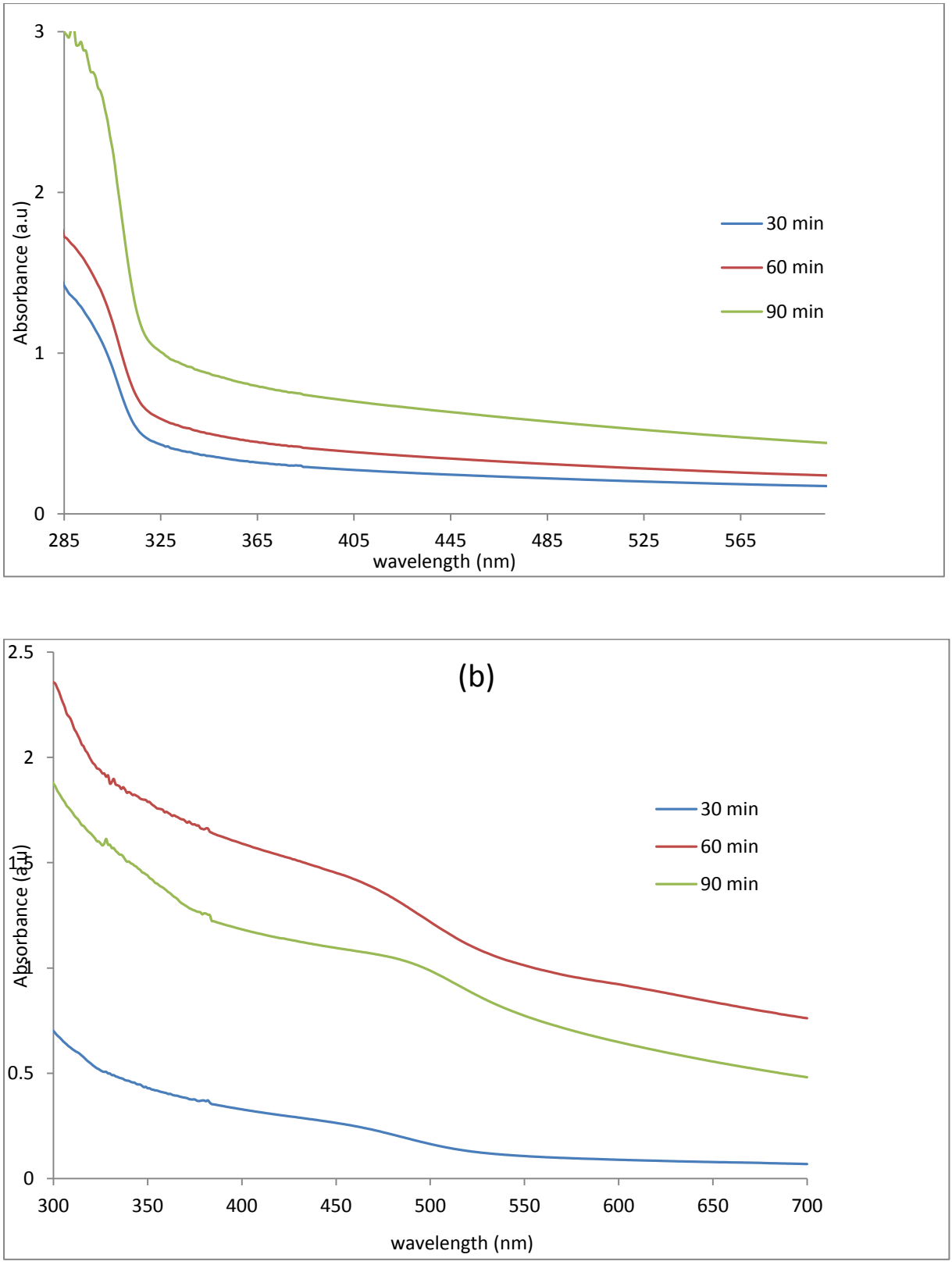

Figure 4. Absorption spectra of (a) ZnS and (b) CdS NPs at different growth time.

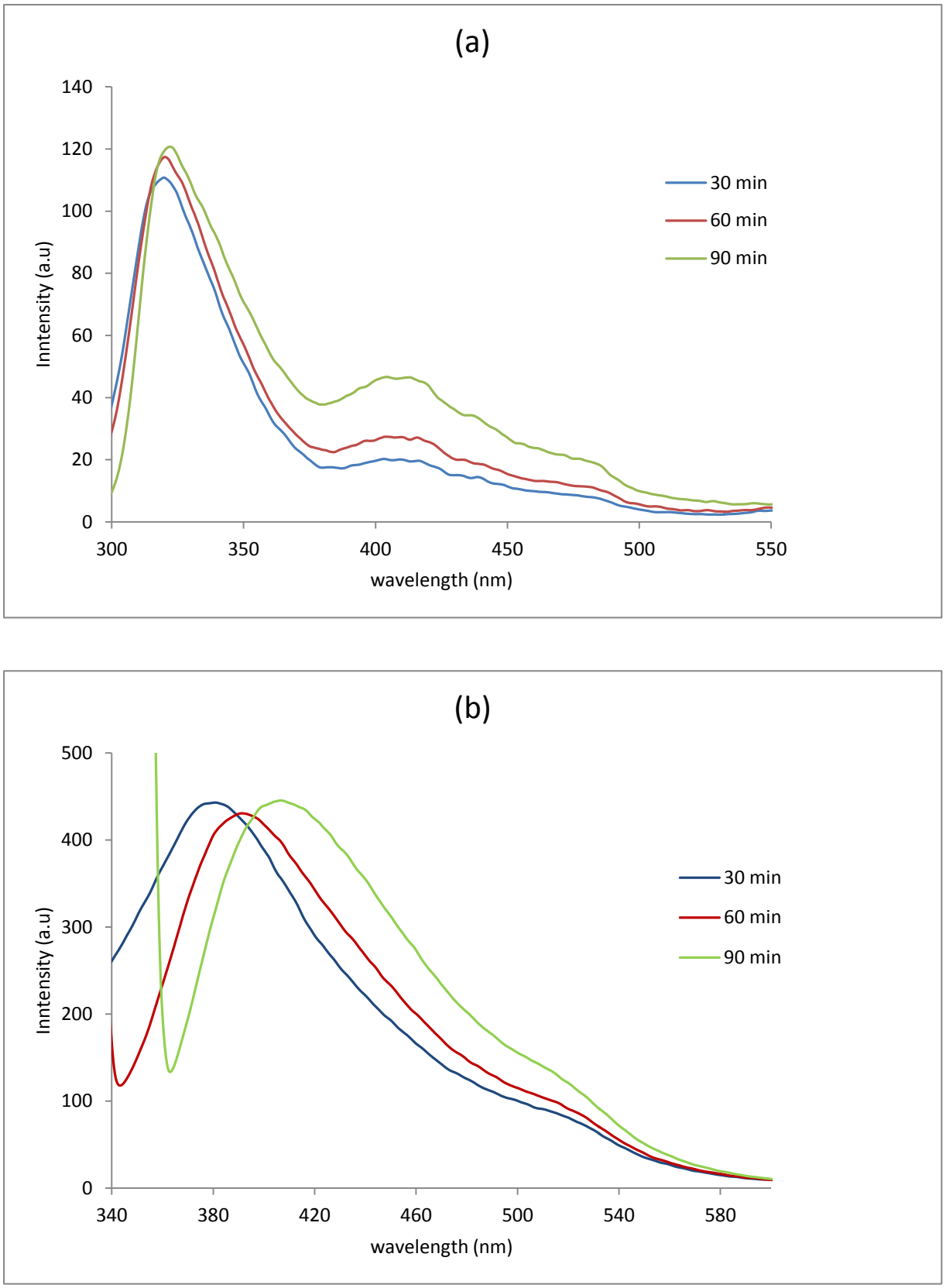

Figure 5. Photoluminescence spectra of (a) ZnS and (b) CdS NPs after different growth times.

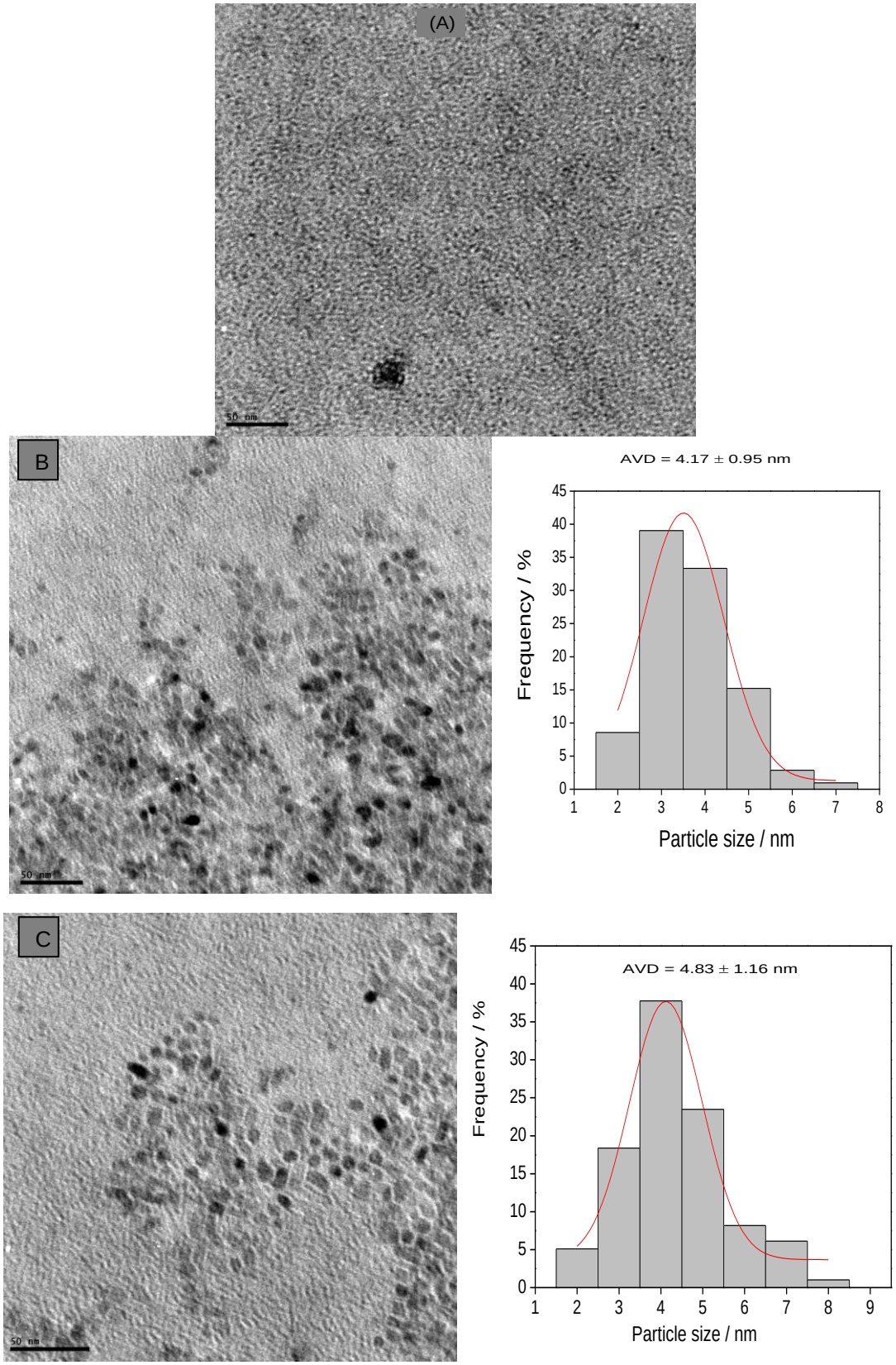

Figure 6. TEM images of ZnS nanoparticles synthesized at 280 °C after (a) 30 min, (b) 60 min and (c) 90 min growth time.

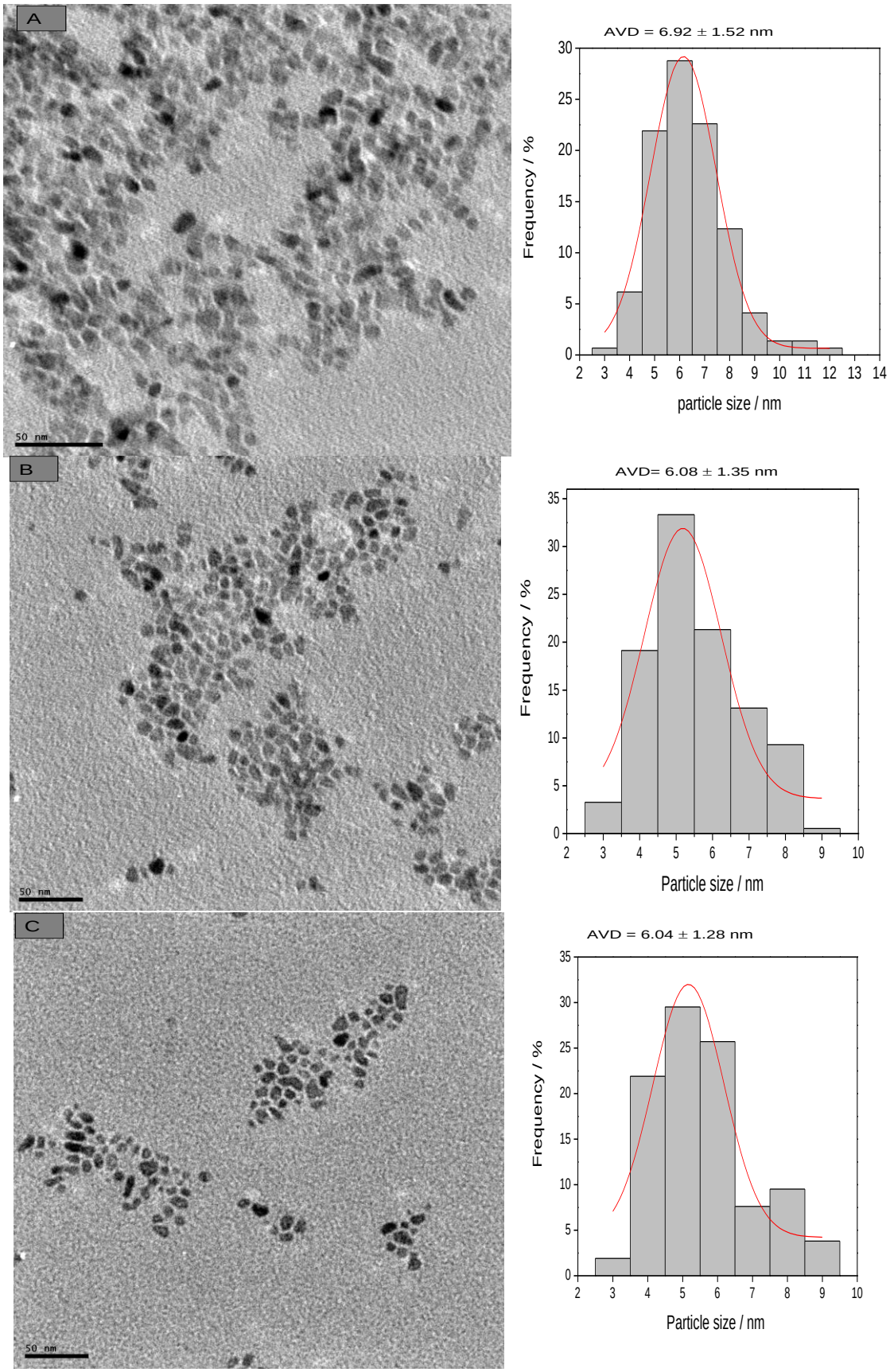

Figure 7. TEM images of CdS nanoparticles synthesised at 268 °C after (a) 30 min, (b) 60 min and (c) 90 min growth time.

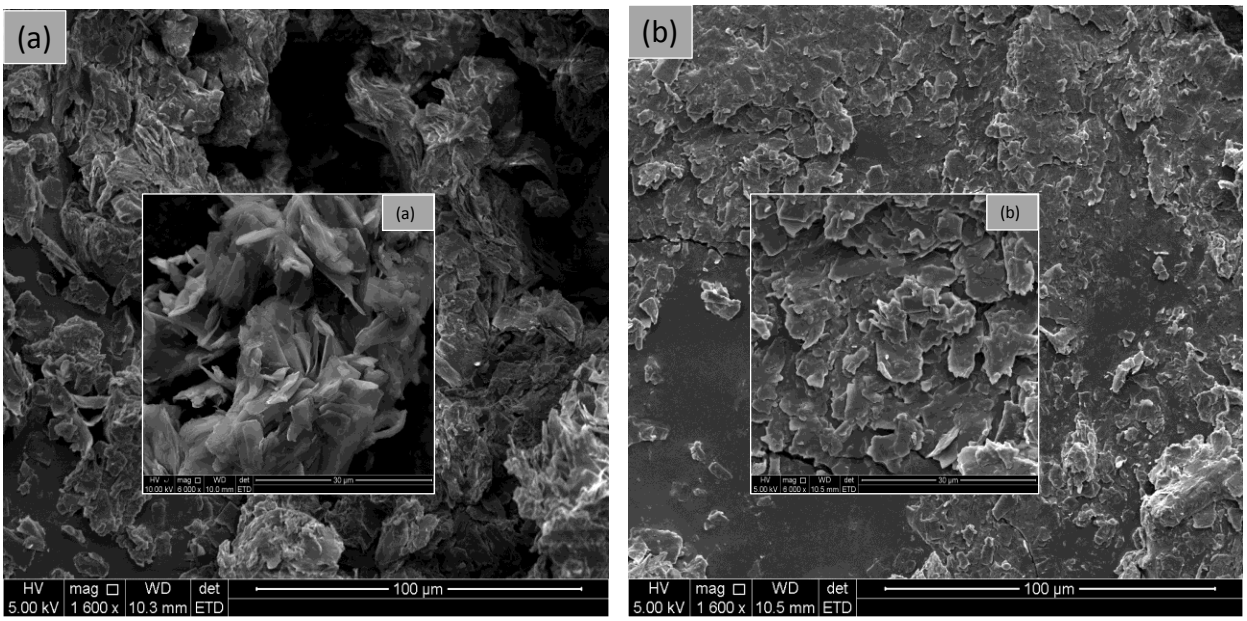

Figure 8. SEM images of ZnS nanoparticles synthesised at 280 °C after (a) 30 min, and (b) after 90 min growth time (insets are higher magnification images).

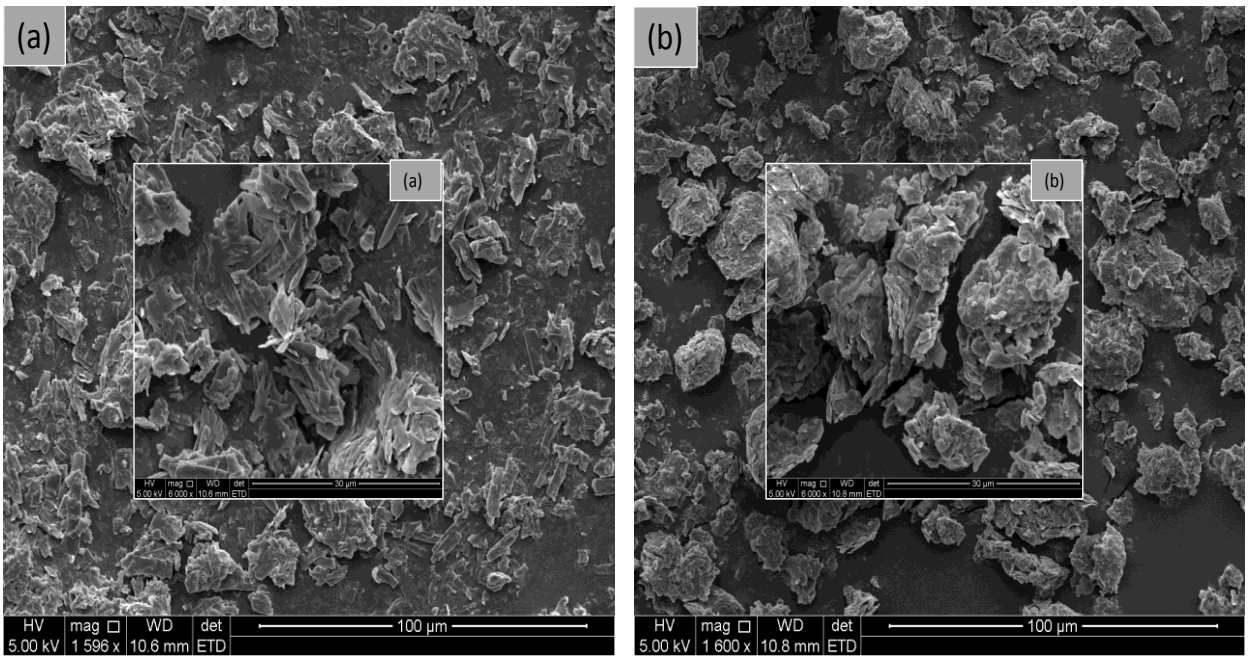

Figure 9. SEM images of CdS nanoparticles synthesised at 265 °C after (a) 30 min, and (b) after 90 min growth time (insets are higher mag. images).

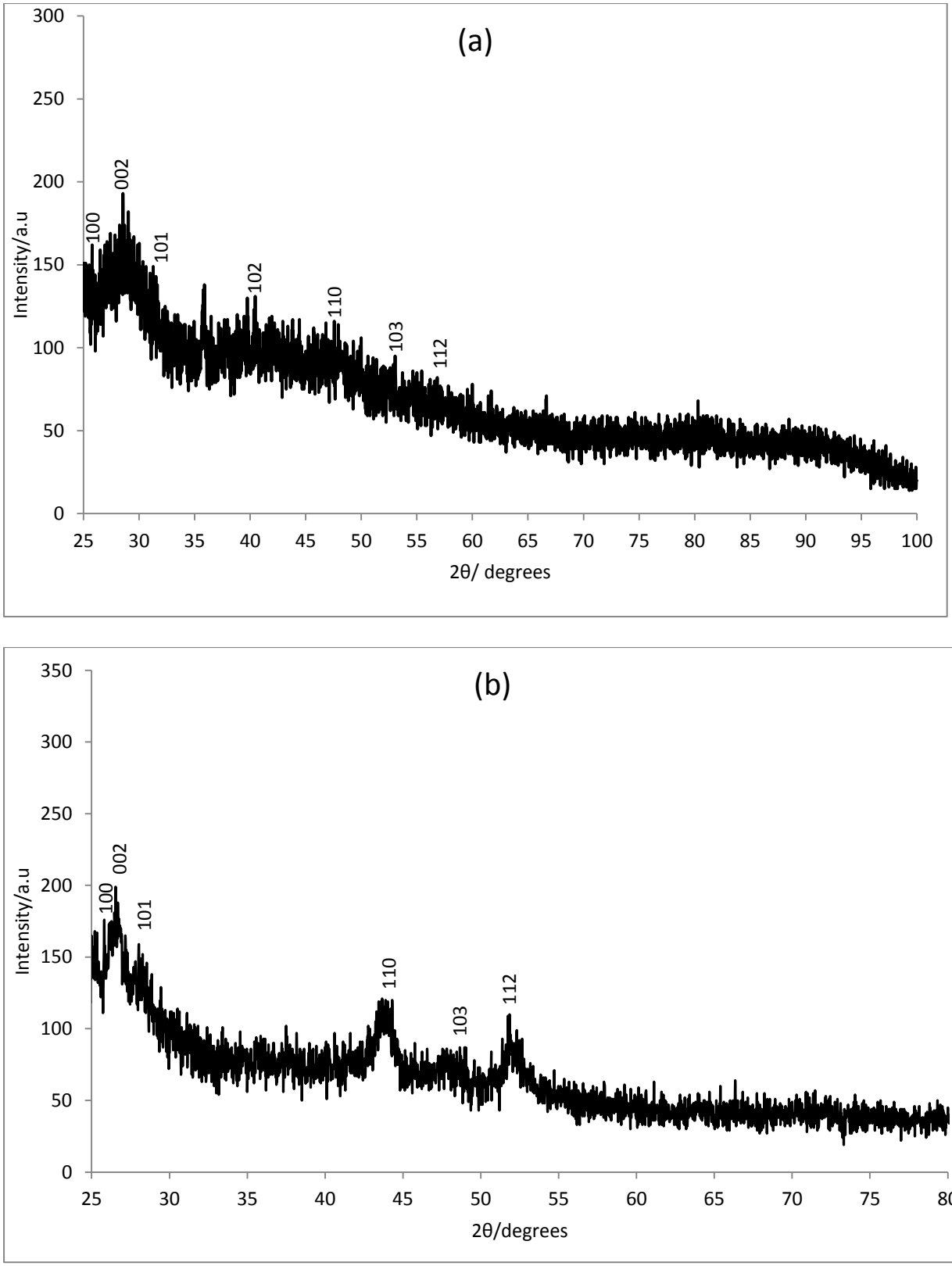

Figure 10. Typical p-XRD patterns of (a) ZnS NPs, and (b) CdS NPs synthesised from [ZnL_2py] and [CdL_2py], at 280 and 268 °C respectively.

Table 1 Crystallographic and refinement parameters

Compound	$[ZnL_2py]$
Color	Colourless platelet
Formula	C23 H25 N3 S4 Zn
Formula mass	537.07
Crystal system	trigonal
Space group	P3121
a (Å)	8.608 (5)
b (Å)	8.608 (5)
c (Å)	29.162(5)
α (°)	90
β (°)	90
γ (°)	120
V ($Å^3$)	1871(3)
Z	3
D_{calc} (g/cm^3)	1.430
Reflections collected	11163
Unique reflections (R_{int})	3082 (0.016)
No. observations (I>2.00σ(I))	2910
No. variables	164
R, wR2	0.0230, 0.0535
GOF	1.07
CCDC number	935369

Table 2: Selected bond length (Å), and bond angles (°) for compound [ZnL_2py]

Bond Length [ZnL_2py] (Å)		Bond Angles [ZnL_2py] (°)	
Zn(1)—N(2)	2.061(3)	S(1)—Zn(1)—S(2)	72.55(2)
Zn(1)—S(1)	2.3583(15)	S(1)—Zn(1)—N(2)	108.02(2)
Zn(1)—S(2)	2.6047(17)	S(1)—Zn(1)—$S(1)^i$	143.96(2)
Zn(1)—$S(1)^i$	2.3583(15)	S(1)—Zn(1)—$S(2)^i$	96.85(2)
Zn(1)—$S(2)^i$	2.6047(17)	S(2)—Zn(1)—N(2)	106.97(8)
C(1)—N(1)	1.336(4)	$S(1)^i$—Zn(1)—S(2)	96.85 (2)
C(2)—N(1)	1.559(8)	S(2)—Zn(1)—$S(2)^i$	146.05(2)
C(4)—N(1)	1.488(9)	$S(1)^i$—Zn(1)—N(2)	108.02(2)
C(11)—N(1)	1.443(3)	$S(2)^i$—Zn(1)—N(2)	106.97(8)
		$S(1)^i$—Zn(1)—$S(2)^i$	72.55(2)

Table 4. Result from TG/DTG and DSC curves for the compounds

Compounds	**[ZnL$_2$py]**		**[CdL$_2$py$_2$]**	
Decomposition stages	First stage	Second stage	First stage	Second stage
Temperature range of decomposition (^{o}C)	150 - 185	201 - 380	66 - 142	212 - 320
DTG peak maximum T(^{o}C)	176	277	105, 123	265
DSC peak: T at maximum peak height(^{o}C)	176	280	107	266
Melting point	201		252	
Mass loss (%) Found Calculated	 14.80 14.70	 79.60 78.70	 23.10 23.80	 70.80 71.40

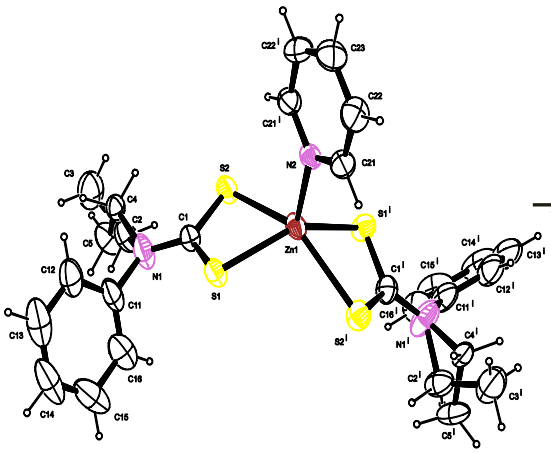

Thermolysis
280 °C/1h